PROCEEDINGS OF SCIENCE

The dynamics of Globular Clusters with the GAIA Data

Marco Merafina*

Department of Physics, University of Rome "La Sapienza",
Piazzale A. Moro 5, I-00185 Rome (Italy)

E-mail: marco.merafina@roma1.infn.it

Statistical analysis on Milky Way globular clusters distribution allows to get the critical value of the onset of gravothermal catastrophe, connected with the maximum of the distribution function. This result, showing that such instability onsets earlier than commonly believed, is confirmed by theoretical calculations taking into account the presence of the effective potential which describes the effects of the tidal forces induced by the hosting galaxy. N-body simulations also confirm the presence of the effective potential with the predicted analytical behavior. With the observational data by the third release of Gaia mission we are now able to recognize the presence of the effective potential in real clusters. Here we present the results for NGC6121 which confirm the theoretical prediction even if in preliminary form.

Multifrequency Behaviour of High Energy Cosmic Sources XIV (MULTIF2023)
12-17 June 2023
Palermo, Italy

*Speaker

PoS(MULTIF2023)013

1. Introduction

It is well known that dynamical evolution of globular clusters (GCs) is strongly affected by collisions among the stars, making favourable a statistical mechanics approach in order to study this important phenomenon. GCs are stellar systems with masses within the interval $10^4 - 10^6\ M_\odot$, containing a number of stars of the order of 10^5 [1]. For their spherical symmetry, there is the possibility to test the evolution of a GC by studying a classical single mass King model [2] in relation to the thermodynamical instability phenomena.

In the evolution of the GCs, stellar encounters strongly contribute in phase space mixing of stellar orbits and thermodynamics plays a central role in the gravitational equilibrium and stability of these clusters, being the average binary relaxation time shorter than their old absolute age which ranges between 10 to 13 Gyr.

On the other hand, the observations of the luminosity profiles of different GCs [3] show similar curves depending only on different values of the star concentration, giving the possibility to fit them by an empirical law and suggesting a unique distribution function for the whole sample of clusters.

Thus, the evolution of the GCs can be simulated by a sequence of thermodynamic equilibrium configurations with different equilibrium parameters, [4] as small thermodynamic transformations which keep constant the functional form of the velocity distribution of stars like in the framework of Boltzmann statistical mechanics, with the relevant difference that the nature of collisions is described in the Fokker-Planck approximation. The gravitational equilibrium models are completely equivalent to ones obtained by King [2], but in the analysis of the thermodynamical instabilities we shall find important innovations, relevant for the evolution of the GCs.

Numerical simulations are also an important and powerful tool to check the validity of the theoretical models, but they enforce us to many limitations. Time of calculus is one of the most significant because simulating N-body systems with $10^5 \div 10^6$ stars requires several months of computing time if one have not a very powerful calculator [5]. We need to simplify our work by making assumptions which sometimes keep us away from studying all the phenomena occurring in the reality and therefore it is necessary to think new ways of implementing cluster models to be able to take into account as many aspects as possible.

Finally, with new observational data (GAIA third data release) we are able to measure velocity components of stars in a systematical way in order to better comprehend kinematics and dynamics of GCs and test the theoretical predictions as well as the N-body simulations results.

2. The observed GCs population and the new Fokker-Planck solution

The problem arises from the open question, not solved for forty years, on the distribution of Milky Way (MW) globular clusters with respect to the critical point related to the onset of the gravothermal catastrophe [6]. This question was firstly outlined by Katz [7] with the comparison of the value of the central gravitational potential (W_0=6.9) corresponding to the maximum of the GCs distribution, with the value (W_0=7.4) corresponding to the onset of gravothermal catastrophe. These values are expected to be coincident because GCs had enough time to undergo the gravothermal catastrophe and, therefore, the distribution of GCs in terms of W_0 should peak exactly in correspondence to the critical value. In fact, the primeval Gaussian distribution, approaching the

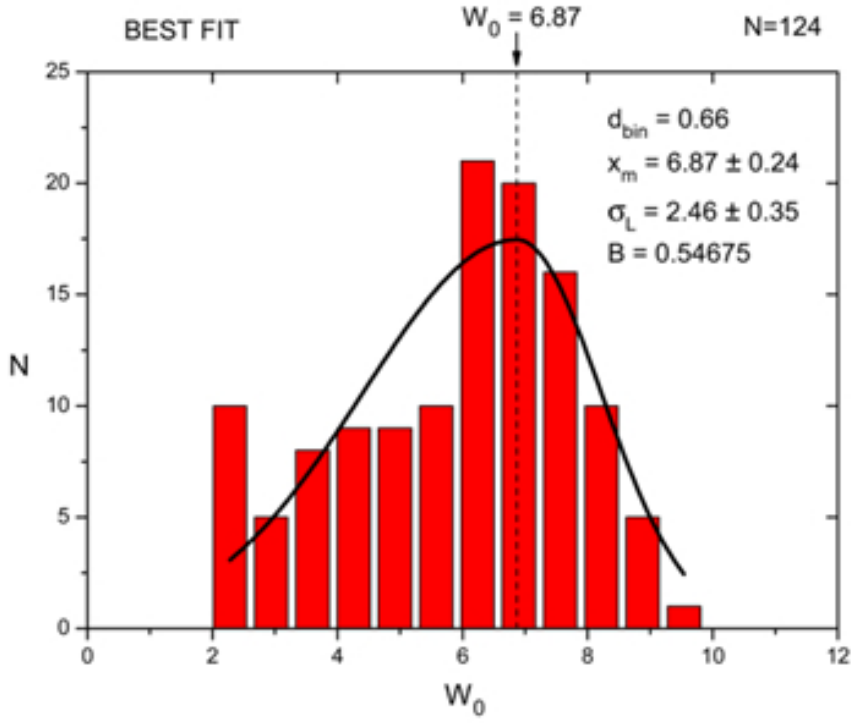

Figure 1: MW GCs distribution at different values of W_0 based on the latest edition (2010) of the Harris Catalogue [8, 9]. Here we considered only 124 objects on a total of 157. The maximum of the curve shows a value of $W_0 = 6.87$. The parameter B is connected with the skewness of the curve.

critical value during the evolution, deforms in a non-symmetric Gaussian curve due to the effect of gravothermal catastrophe which progressively subtracts the collapsed GCs with values of W_0 larger than the critical value. For these reasons, the resulting distribution must present a maximum which corresponds to the onset of gravothermal instability. Nevertheless the values are significantly different and also the new data from Harris Catalogue on MW GCs (157 objects) [8] do not contribute to the solution of the problem (see Fig.1).

In order to understand if the onset of gravothermal catastrophe is correctly performed, we reconsider the solution of the Fokker-Planck equation, starting from the assumption that the distribution in energy must have a Boltzmann form to correctly define the entropy as the logarithm of the statistical weight of macroscopic states. For solving the equation in terms of Hamiltonian of the single star, we consider the Fokker-Planck equation in the form introduced by Spitzer & Harm [10]

$$\frac{d}{dx}\left[G(x)\left(\frac{dg(x)}{dx}+2xg(x)\right)\right]+\lambda x^2 g(x)=0\,, \tag{1}$$

where

$$G(x)=\frac{4}{\sqrt{\pi}x}\int_0^x e^{-y^2}y^2dy\,, \tag{2}$$

while $x = v/\sqrt{2}\sigma$ and $\sigma = \sqrt{k\theta/m}$ are the dimensionless velocity and the Boltzmann velocity dispersion, respectively. θ is the thermodynamic temperature. The parameter λ is the fractional loss rate of the stellar evaporation suffered by the cluster. [11]

We search a solution of the form $g(x) = Ae^{-H(x)/k\theta}$, where $H(x) = H_0(x) + H_1(x)$ is the Hamiltonian of the single star and $H_1(x) = 0$ when $\lambda = 0$. So that, being $\lambda \ll 1$, we can write at the first order

$$\exp\left[-H_1(\lambda, x)/k\theta\right] \simeq 1 - \frac{\lambda}{k\theta}\frac{\partial H_1}{\partial \lambda}\bigg|_{\lambda=0} . \tag{3}$$

Inserting $g(x)$ in Eq.(1), equating the terms with the same power of λ and neglecting the higher order terms to λ we obtain

$$\frac{\partial H_1}{\partial \lambda}\bigg|_{\lambda=0} = \frac{\sqrt{\pi}}{8} k\theta \left(e^{x^2} - 1\right) , \tag{4}$$

and, finally, we get the Hamiltonian form as

$$H(x) = k\theta\left\{x^2 - \ln\left[1 - \frac{\sqrt{\pi}}{8}\lambda\left(e^{x^2} - 1\right)\right]\right\} . \tag{5}$$

The logarithmic term in Eq.(5) is the effective potential which takes into account of the tidal forces induced by the hosting galaxy. In absence of evaporation of the stars of the cluster ($\lambda = 0$) this term reduces to zero.

3. Discussion

With the resolution of the Fokker-Planck equation we obtained in the Hamiltonian of the distribution an additional term, named “effective potential", which is the effect of the equilibrium established by two competitive processes: one due to collisions among stars with an exchanging of energy which tends to modify the distribution by driving it to the Boltzmann one with the formation of a tail at large energy; one, in opposition, due to evaporation of stars as result of the presence of tidal forces induced by the hosting galaxy that removes continuously the stars and prevents the formation of the tail, maintaining a cutoff energy and a limited phase space. These two competitive effects keep unchanged the form of the energy distribution function during the dynamical evolution of the GCs, namely that we can consider as a “thermodynamical equilibrium" from the astrophysical point of view, with the collisions ruled by the Fokker-Planck approximation. The presence of the effective potential do not affect the internal dynamics of stars and sum of kinetic and gravitational energy remains constant in the motion between two consecutive collisions, as well the effective potential. The result is that the Hamiltonian (total energy) remains a constant of motion and the dynamical problem of the single mass orbit keep unchanged. Nevertheless, the presence of the effective potential has important consequences from the thermodynamical point of view resulting in the formation of regions with negative and positive specific heat which guarantee the evolution of the system towards the gravothermal instability [12].

Moreover, the additional (positive) contribution of the effective potential on the total energy $E_{tot} = E_{kin} + E_{gr} + E_{eff}$, considering also the virial condition $2E_{kin} + E_{gr} = 0$, implies that $E_{tot} = -E_{kin} + E_{eff}$. This term affects the caloric curve and change the critical point of the onset of gravothermal instability to a value which corresponds to the maximum of the GC distribution (from W_0=7.4 to W_0=6.9) [13], as initially requested. The open question appears to be definitely solved taking into account the effects due to the presence of the effective potential. These results are shown in Fig.2.

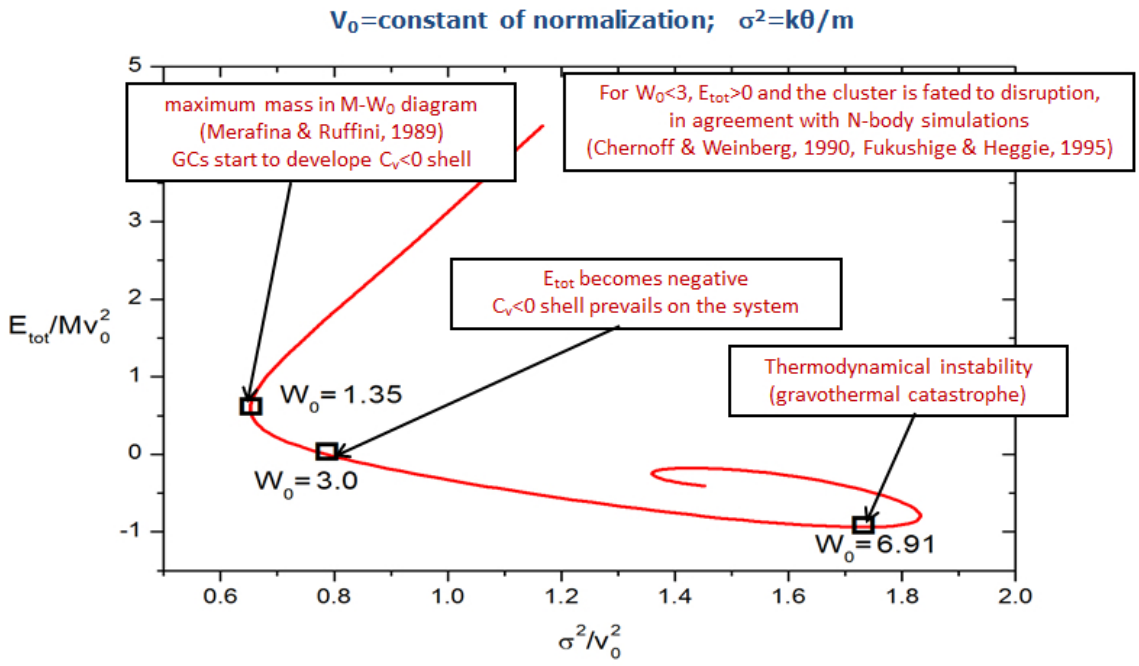

Figure 2: Caloric curve with the presence of the effective potential. The main theoretical results are highlighted with labels (see [14–16]). The theoretical value corresponding to the onset of gravothermal catastrophe now is compatible with the statistical analysis based on Harris Catalogue [8, 9].

Another important result derived by this treatment is the threshold at $W_0 = 3$ corresponding to the zero total energy. Clusters with lesser values of W_0 are fated to disruption, because the tidal forces are prevalent to the gravitational ones. This result can explain observational data and N-body simulations going to the same conclusions [15, 16].

A different analysis about the thermodynamic stability, extended to the relativistic regime for models not including effective potential, was also developed by Bisnovatyi-Kogan & Merafina [17]. Here, the results were related with ones concerning the dynamical stability in a more general framework.

Finally, it could be useful to take into account of other observational evidences that confirm the onset of instability at the value just mentioned, by considering the behavior of the central relaxation time t_{rc} [18] and the core-collapse time t_{cc} [19] on the basis of the data obtainable from the Harris Catalogue. These evidences are reported in the Fig.3 and Fig.4.

4. Effective potential and N-body simulations

Before considering the observative data on transverse velocities of stars in GCs, enabling to test the model and the presence of effective potential in real systems, we performed a N-body simulation for two model with $N = 32768$ and $N = 262144$ stars, respectively. In order to extract some information valid for the entire cluster, we considered the total energy E as sum of the gravitational and kinetic energy of each star and calculated the total number of stars of equal E, comparing the obtained distribution with the one of Boltzmann form with the Hamiltonian H above

$$t_{rc} = \left[\frac{\pi}{\sqrt{2}}\frac{G^2 m \rho_0}{\sigma^3}\ln(N/2)\right]^{-1}$$

$$\log[t_{rc}/1yr] \approx -(0.364 \mp 0.028)W_0 + (10.60 \pm 0.18)$$

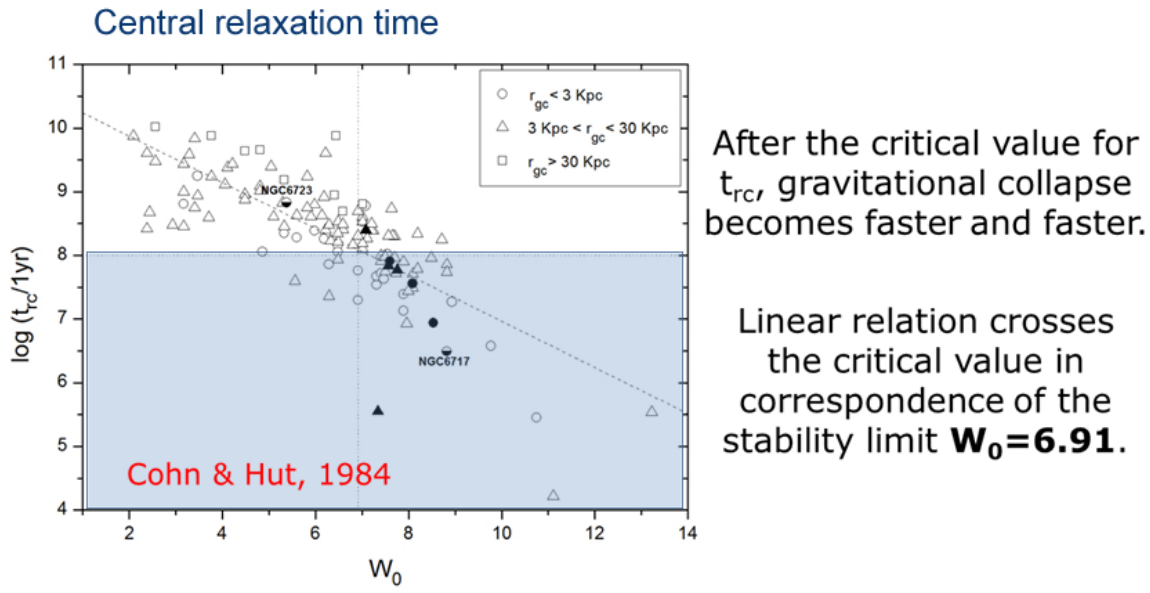

Figure 3: The time-scale t_{rc} by using Harris Catalogue Data [8, 9] and the results of the analysis carried out by Cohn & Hut [18].

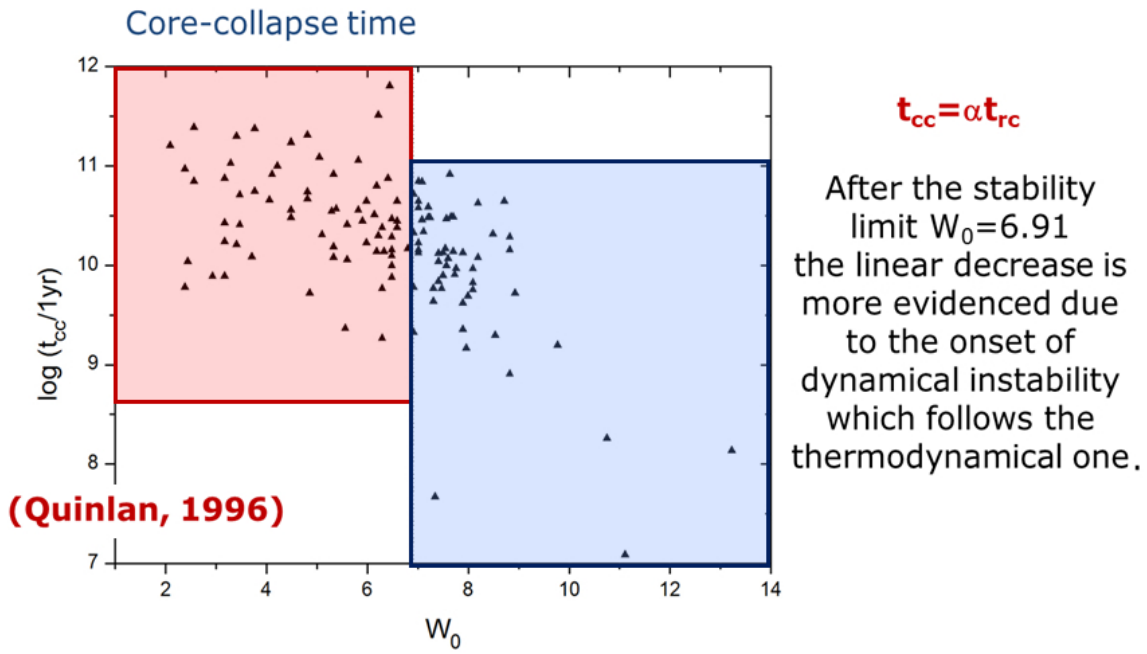

Figure 4: The time-scale t_{cc} by using data by Quinlan [19].

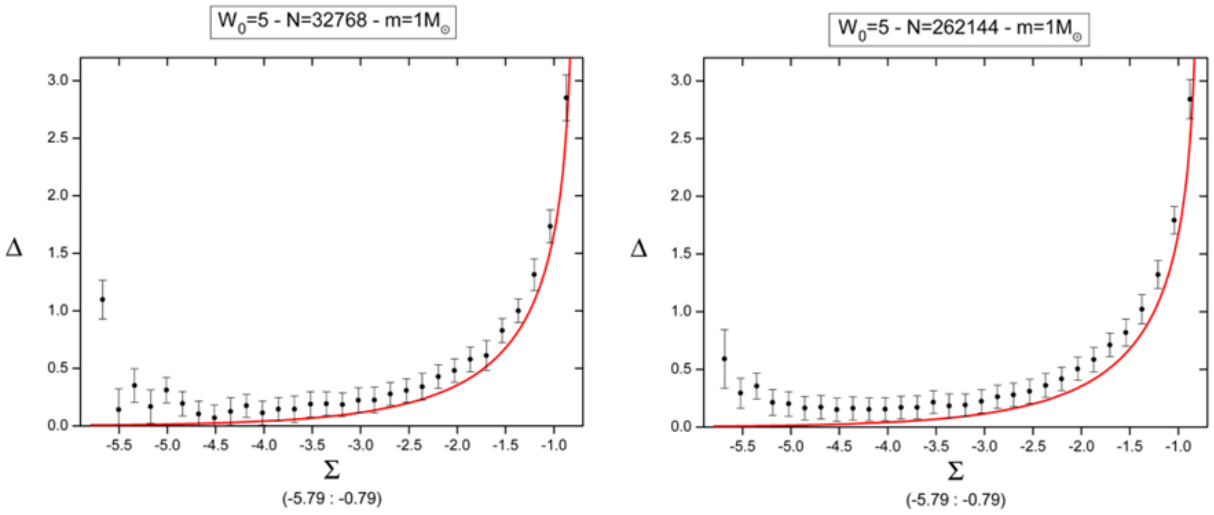

Figure 5: Effective potential by the N-body simulations with $N = 32768$ and $N = 262144$ stars. The continuous curve represents the theoretical prediction.

carried out. The number of stars at fixed energy E is also proportional to $e^{-H/k\theta}$ and therefore we are able to obtain the value of H for each value of E through the number of stars. In addition, we have that $H = E + m\psi$, where ψ is the effective potential. Thus, in terms of dimensionless quantities, being $\Omega = H/k\theta$, the effective potential $\Delta = m\psi/k\theta$ can be expressed, starting from Eq.(5), as

$$\Delta = -\ln\left(1 - e^{\Sigma - W_\infty}\right) , \tag{6}$$

where $W_\infty = m\phi_R/k\theta$ is the dimensionless form of the gravitational potential at the surface of the cluster, while $\Sigma = E/k\theta$ is the dimensionless sum of the gravitational and kinetic energy of a single star. Furthermore, $\Omega = \Sigma + \Delta$ and then, using the number of stars at fixed Σ allows to obtain the value of Ω and, consequently, the effective potential Δ by subtracting kinetic and gravitational energy Σ to the value of Ω. The results are summarized in Fig.5.

We obtained a very good accordance with the expected curve. The small disagreement is due to the transition from continuous (theory) to discrete (N-body simulation) system, depending on the choice of the radial-energy mesh for individuating the sample of stars with same energy. This disagreement becomes more relevant at low energies, especially at the center of the cluster, for lack of stars at zero kinetic energy.

5. The GAIA Data Release 3

With the GAIA mission [20] we have a large amount of data available that allow us to develop an analysis of the stellar kinematics of a globular cluster which was not previously possible, through the use of data on the transverse velocities of the stars. The informations on the number of sources considered in this release [21], compared and contrasted with ones of the previous releases and the physical characteristics used in our analysis are summarized in Fig.6. Our preliminary choice has been the globular cluster NGC6121.

https://www.cosmos.esa.int/web/gaia/dr3 Gaia Data Release 3 contents summary - Gaia - Cosmos

	# sources in Gaia DR3	# sources in Gaia DR2	# sources in Gaia DR1
Total number of sources	**1,811,709,771**	**1,692,919,135**	**1,142,679,769**
	Gaia Early Data Release 3		
Number of sources with full astrometry	1,467,744,818	1,331,909,727	2,057,050
Number of 5-parameter sources	585,416,709		
Number of 6-parameter sources	882,328,109		
Number of 2-parameter sources	343,964,953	361,009,408	1,140,622,719
Gaia-CRF sources	1,614,173	556,869	2191
Sources with mean G magnitude	1,806,254,432	1,692,919,135	1,142,679,769
Sources with mean G_{BP}-band photometry	1,542,033,472	1,381,964,755	-
Sources with mean G_{RP}-band photometry	1,554,997,939	1,383,551,713	-

Gaia table name	Unit	Description
parallax	$[mas]$	Absolute parallax of the source
parallax_error	$[mas]$	Standard error of the parallax
ra, dec	$[deg]$	Barycentric right ascension α in ICRS
dec	$[deg]$	Barycentric declination δ in ICRS
ra_error	$[deg]$	Error associated to the coordinate α
dec_error	$[deg]$	Error associated to the coordinate δ
pmra	$[mas/yr]$	Proper motion $\mu_{\alpha*} = \mu_\alpha \cos\delta$ in the RA direction
pmdec	$[mas/yr]$	Proper motion μ_δ in declination
pmra_error	$[mas/yr]$	Error in the proper motion data $\mu_{\alpha*}$
pmdec_error	$[mas/yr]$	Error in the proper motion data μ_δ
radial_velocity	$[km\,s^{-1}]$	Spectroscopic RV in the Solar System reference frame
radial_velocity_error	$[km\,s^{-1}]$	Error associated to RV data

Data used for our research

(in collaboration with Pietro Ferraiuolo)

Searching for velocity components of stars in globular clusters

First choice: NGC6121 (preliminar analysis)

Name of GC	RA [deg]	DEC [deg]	R_c [deg]	R_{scan} [deg]	$\log c$	W_0	Nr source (Raw)	Nr with $\bar{\omega} > 0$ ($v_{rad} \neq 0$)
NGC6121	245.89	-26.52	0.019	0.193	1.65	7.41	27823	23988 (499)

Figure 6: GAIA Data Release 3: some general informations [20, 21].

Position: very close to Antares, Galactic plane

Concentration: c=1.65 (W_0=7.41)
Tidal Radius: R_t=27.9 pc
Core Radius: R_c=0.62 pc
Mass: M=9.04·10^4 $M_\odot$
Distance from Sun: $d_\odot$ =1.85 kpc
Galactocentric distance: D_G=6.45 kpc

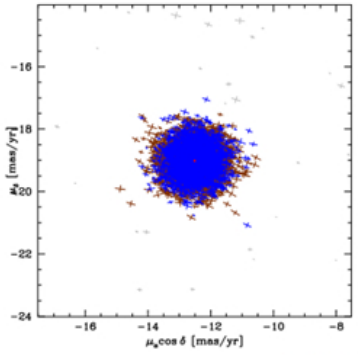

Proper motion

Radial velocity

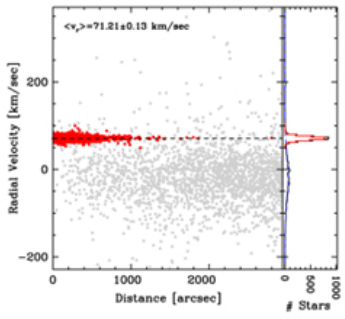

https://people.smp.uq.edu.au/HolgerBaumgardt/

Figure 7: Main features of NGC6121 [22].

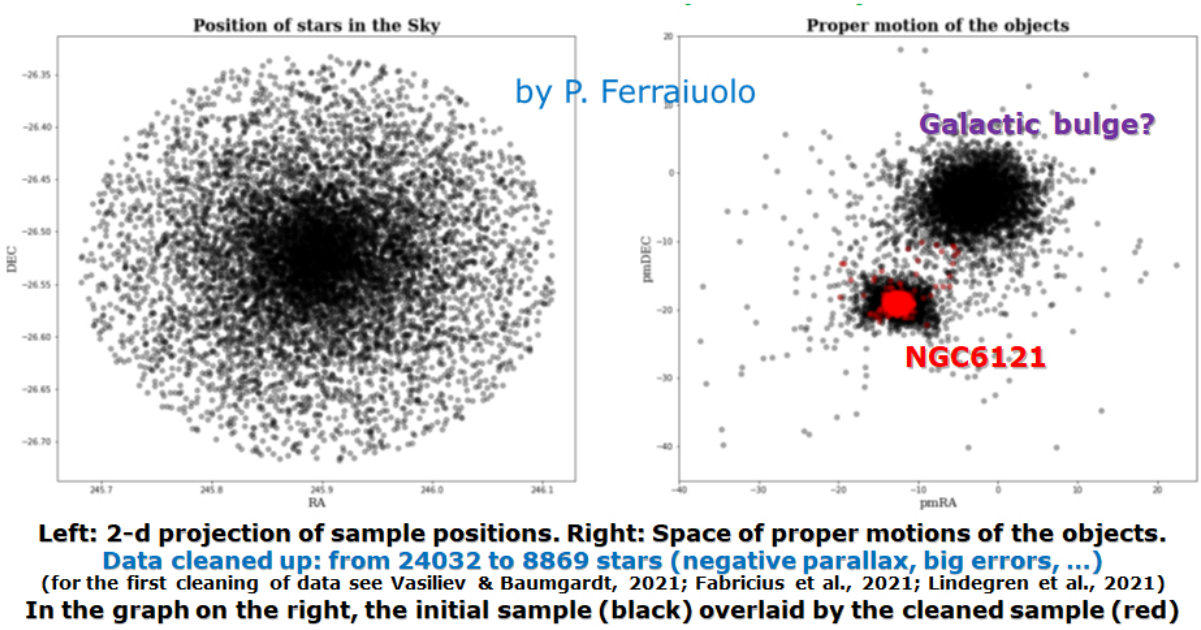

Figure 8: Preliminary plot for obtaining a sample of stars with velocity components [23–25].

In Fig.7 the main features of NGC6121 together with the data on the proper motion and radial velocity useful for developing our analysis on kinematics of the stars belonging to this cluster are summarized. Our goal is to demonstrate the existence of effective potential in real clusters and to get its behavior to compare with the theoretical prediction. The preliminary sample with positions of stars of the clusters and their proper motions is shown in Fig.8. We note a difficulty in the individuation of data belonging to clusters due to the presence of stars which presumably belong to the galactic bulge. The sample was also cleaned in order to take into account of the presence of data with negative parallax or big relative errors. At the end of this procedure the number of stars decreased from 24032 to 8869 [23–25].

6. Kinematics in NGC6121

In order to obtain informations about the characteristics of the star velocity distribution in NGC6121, it is important to analyze the distribution of the different components of the velocity of any star belonging to cluster. Starting from the cleaned sample, the request to include only the stars up to the tidal radius R_t of NCG6121 gives us a strong reduction of the number of star, also due to the availability of the three components of the velocity. We arrive to 726 stars. Moreover the unsatisfactory sample of the radial component v_r^2, with only 82 stars, forces us to make use of the isotropy condition on the velocity distribution to make up for the lack of data on radial velocities (see Fig.9). Thus we can obtain

$$v^2 = \frac{3}{2}(v_x^2 + v_y^2)\,, \tag{7}$$

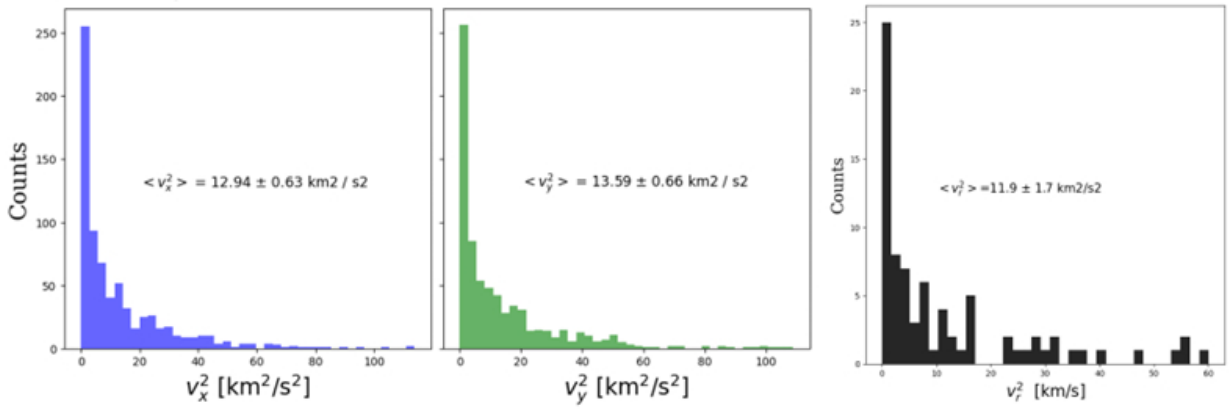

Figure 9: The components of the squared velocity of the stars in NGC6121. We note a poorly distribution of radial velocities. The averages $\langle v^2 \rangle$ of the single components are also indicated.

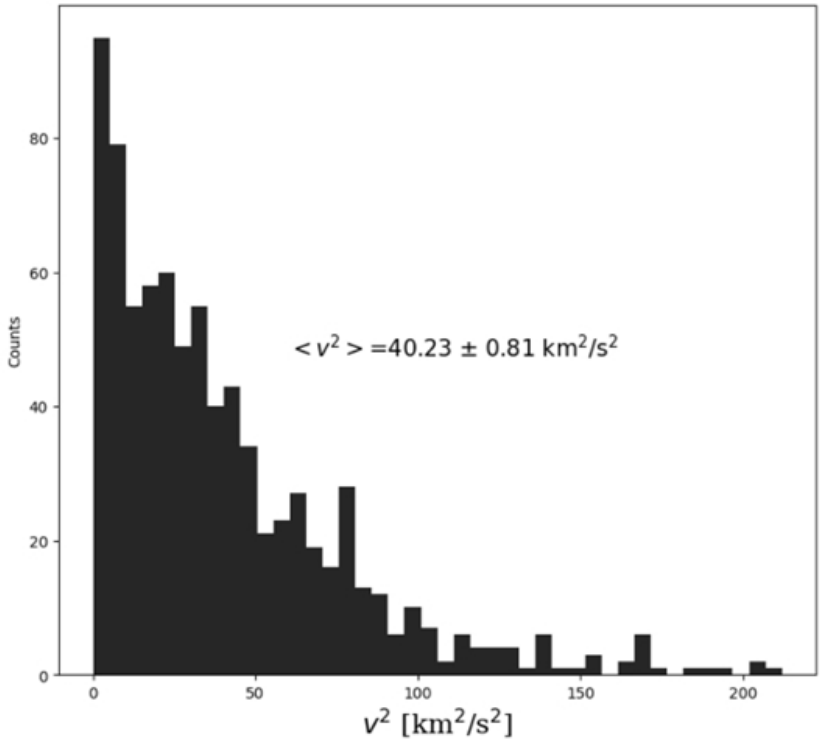

Figure 10: Squared velocity distribution of stars in NGC6121.

with the statistics remaining unchanged. The final data are given in Fig.10. Unfortunately the sample is largely incomplete, and the difficulty to calculate the gravitational potential for each star suggests to consider only a single shell at fixed distance r in order to have the same value of the gravitational potential (rough approximation) for all the stars. We choose a shell at 15.45 pc away from the center of the cluster. The new distribution of star is given in Fig.11.

The characteristics of the King model describing NGC6121 permit to get the value of many parameters of the cluster. From Harris Catalogue, we have that $W_0 = 7.41$, the tidal radius is

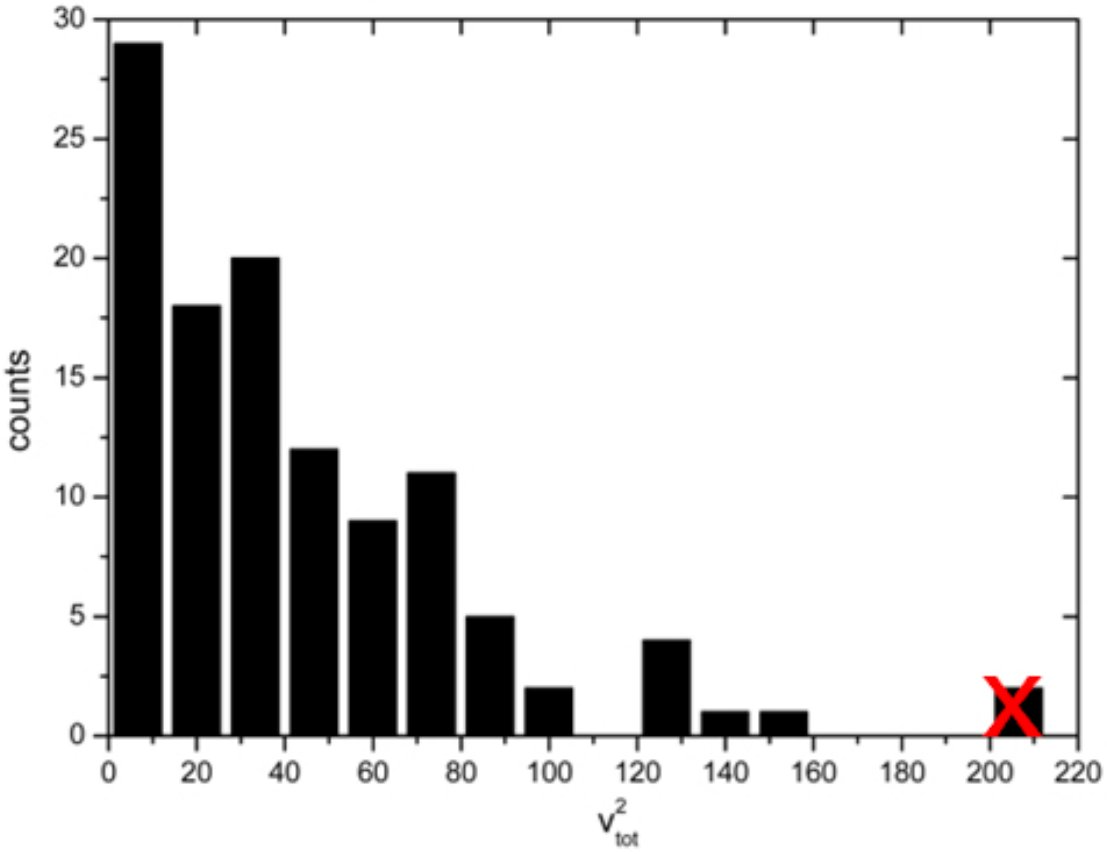

Figure 11: Squared velocity distribution of stars at r =15.45 pc.

R_t = 27.9 pc and, for r = 15.45 pc, the King ratio r/R_t is equal to 0.554 which corresponds to $W(r)$ = 0.3819. From the squared velocity distribution of Fig.11, where we have excluded the last data beyond 200 km^2/s^2, we have a maximum value v^2_{max} = 159.9 km^2/s^2, used to get the squared velocity dispersion σ^2 by the relation $W(r) = v^2_{max}/2\sigma^2$. The value obtained is σ^2 = 209.35 km^2/s^2 corresponding to σ = 14.47 km/s. Again, the new sample is poorer of stars ($N = 114 - 2$), then we assume the reduction of the sample to be not selective and therefore, the number of stars in the sample ΔN^* can be considered as simply connected with the total number of stars populating the shell ΔN by the relation

$$\Delta N^* = \alpha \Delta N \,, \tag{8}$$

with $\alpha < 1$.

Now we are able to calculate the effective potential in the single shell at r = 15.45 pc, assuming constant the gravitational potential $m\varphi$. Being

$$\frac{\Delta N}{\Delta V} = \frac{\Delta N^*}{\alpha \Delta V} = f \Delta^3 p \,, \tag{9}$$

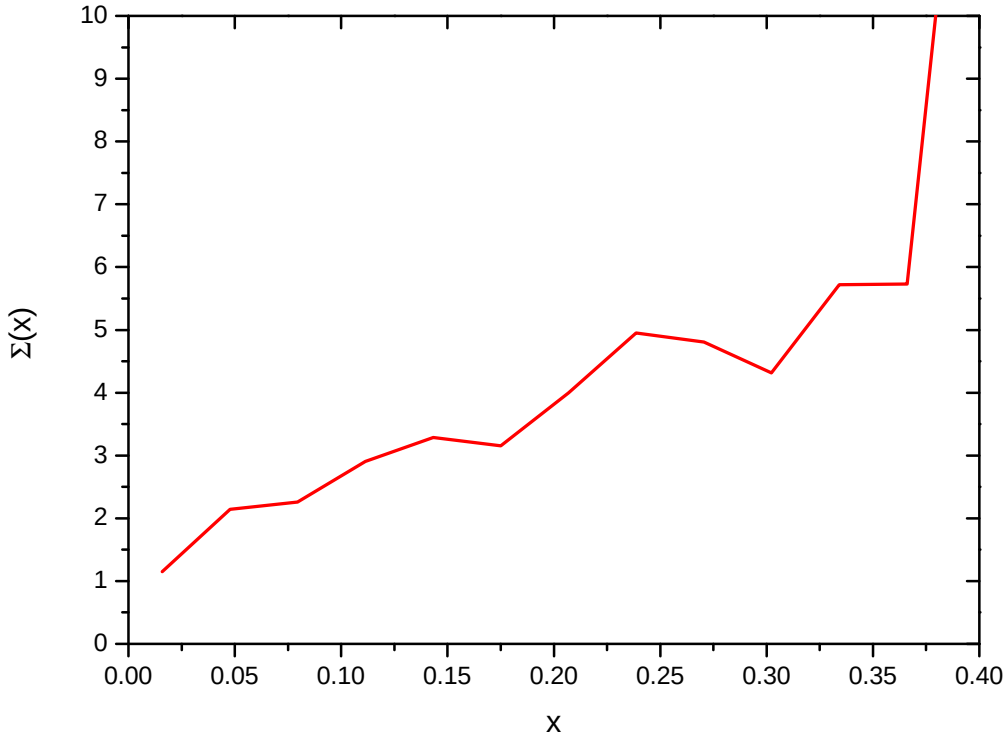

Figure 12: The effective potential in NGC6121 in the shell at 15.45 pc.

with $f = Ae^{-H/k\theta}$ and $H = \varepsilon + m\psi$, where ε is the kinetic energy of the single star and ψ the effective potential, we can introduce the dimensionless quantities $\Omega = H/k\theta$, $\Sigma = m\psi/k\theta$, $x = \varepsilon/k\theta = v^2/2\sigma^2$, $W = \varepsilon_c/k\theta = v^2_{max}/2\sigma^2$, where ε_c is the cutoff kinetic energy and θ, as usual, is the thermodynamic temperature. Since $\Omega = x + \Sigma$, the dimensionless effective potential Σ, with few simple steps, can be rewritten as

$$\Sigma = \text{const} - \ln\left(\Delta N^*/x^{1/2}\right) - x \ . \tag{10}$$

In Fig.12 the behavior of Σ is shown as a function of the dimensionless kinetic energy x to compare with the theoretical prediction of Fig.13. The constant is normalized in order to make equivalent the initial values of both graphs.

7. Conclusions

1. Measurements of transversal star velocities allowing to analyze the real kinematics in globular clusters give the possibility to test theoretical equilibrium models and make possible to verify the existence of the effective potential from observational data, instead of using only numerical simulations. Isotropy in the velocity distribution is verified.

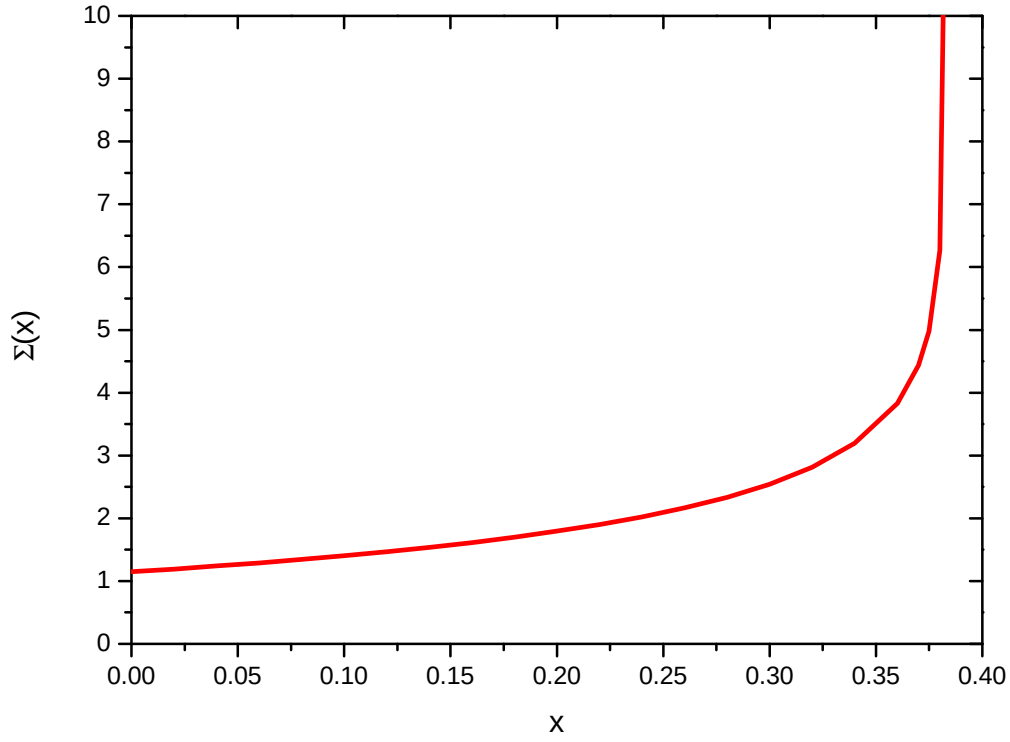

Figure 13: Theoretical behavior of the effective potential.

2. The difficulty to obtain a fully satisfactory profile of the effective potential is due to different factors:

- calculations restricted to a single fixed shell: the incompleteness of data due to this choice (at moment) significantly affects the expected velocity distribution of the stars;

- the assumption that the gravitational potential is constant in the fixed shell;

- the mass of the stars assumed to be constant without considering (at moment) the effects of a mass function;

- the lack of a detailed analysis of the density profile without a suitable sample of data.

3. Nevertheless, a proof of the existence of the effective potential is given also with limited data.

4. We shall improve the work extending the analysis to different shells in the same cluster and considering the cluster in the whole, by using not local parameters and considering also the effect of gravitational potential on the entire cluster: the next system under analysis will be the big cluster NGC104 (47 Tuc).

5. Finally, we will extend the analysis of dynamics of globular clusters with six other clusters from GAIA catalog (NGC4372, NGC5139 (ω Cen), Palomar 5, NGC6656 (M22), GLIMPSE02 and NGC6712) in order to obtain better representations of the effective potential.

References

[1] J. Binney, S. Tremaine, *Galactic Dynamics*, Princeton Univ. Press, Princeton (1987).

[2] I.R. King, AJ **71**, 64 (1966).

[3] I.R. King, AJ **67**, 471 (1962).

[4] G. Horwitz, J. Katz, ApJ **211**, 226 (1977).

[5] A. Sollima, E. Dalessandro, G. Beccari, C. Pallanca, MNRAS **464**, 3871 (2017).

[6] D. Lynden Bell, R. Wood, MNRAS **138**, 495 (1968).

[7] J. Katz, MNRAS **190**, 497 (1980).

[8] W.E. Harris, AJ **112**, 1487 (1996).

[9] W.E. Harris, arXiv:1306.2247v1 (2013).

[10] L. Spitzer, R. Harm, ApJ **127**, 544 (1958).

[11] I.R. King, AJ **70**, 376 (1965).

[12] M. Merafina, D. Vitantoni, Acta Polytechnica CTU Proc. **1**, 231 (2014).

[13] K. Piscicchia, M. Merafina, *Proceedings of the Fourteenth Marcel Grossmann Meeting on General Relativity* **C**, 2515, World Scientific Publishing, Singapore (2018).

[14] M. Merafina, R. Ruffini, A&A **221**, 4 (1989).

[15] D.F. Chernoff, M.D. Weinberg, ApJ **351**, 121 (1990).

[16] T. Fukushige, D.C. Heggie, MNRAS **276**, 206 (1995).

[17] G.S. Bisnovatyi-Kogan, M. Merafina, ApJ **653**, 1445 (2006).

[18] H. Cohn, P. Hut, ApJ **277**, L45 (1984).

[19] G.D. Quinlan, New A **1**, 255 (1996).

[20] T. Prusti, J.H.J. de Bruijne, et al. [The Gaia mission], A&A **595**, A1 (2016).

[21] A. Vallenari, A.G.A. Brown, et al. [Gaia Data Release 3: Summary of the content and survey properties], A&A **674**, A1 (2023).

[22] H. Baumgardt, E. Vasiliev, MNRAS **505** (4), 5957 (2021).

[23] E. Vasiliev, H. Baumgardt, MNRAS **505** (4), 5978 (2021).

[24] C. Fabricius, et al., A&A **649**, A5 (2021).

[25] L. Lindegren, U. Bastian, M. Biermann, et al., A&A **649**, A4 (2021).

DISCUSSION

MATTEO BACHETTI: Can RADIO PULSAR observations help your modeling, either directly or as a benchmark? In principle, their precise timing should allow good radial velocity measurements.

MARCO MERAFINA: The question is not finding a correct position of the stars, but the lack of stars in the sample. Other difficulties arise from the calculation of the gravitational potential in order to enlarge the dimension of the sample by extending the volume from a single fixed shell to the entire cluster. Finally, taking into account the mass function and considering also the presence of neutron stars, white dwarfs and binary systems can contribute to improve the precision of the results. We will take into account these improvements in the analysis of other GCs with better suitable conditions in the relative position with respect to Galaxy (i.e. far from the bulge and the disk of the Galaxy).

MASSIMILIANO DE PASQUALE: How many gravothermal GCs in our Galaxy?

MARCO MERAFINA: The W_0-distribution is skewed for large values of W_0, it shows how many GCs have gone through the gravothermal catastrophe.